AJR FOCUS ON:

Preoperative Diagnosis of Regional Lymph Node Metastasis of Colorectal Cancer With Quantitative Parameters From Dual-Energy CT

Zehong Yang[1,2]
Xiang Zhang[1,2]
Mengjie Fang[3,4]
Guolin Li[2,5]
Xiaohui Duan[1,2]
Jiaji Mao[1,2]
Jun Shen[1,2]

Keywords: colorectal neoplasm, diagnostic imaging, lymphadenopathy, MDCT

doi.org/10.2214/AJR.18.20843

Received October 29, 2018; accepted after revision February 7, 2019.

Supported by Guangdong Province Universities and Colleges Pearl River Scholar Funded Scheme (2017), National Natural Science Foundation of China (grants 81571739, 81371607), Guangdong Natural Science Foundation (grants 2014A030312018, 2017A030313777), National Basic Research Program of China (grants 2015CB755500), and the Elite Young Scholars Program of Sun Yat-Sen Memorial Hospital (J201403).

[1]Department of Radiology, Sun Yat-Sen Memorial Hospital, Sun Yat-Sen University, 107 Yanjiang Rd W, Guangzhou 510120, China. Address correspondence to J. Shen (shenjun@mail.sysu.edu.cn).

[2]Guangdong Provincial Key Laboratory of Malignant Tumor Epigenetics and Gene Regulation, Medical Research Center, Sun Yat-Sen Memorial Hospital, Sun Yat-Sen University, Guangzhou, China.

[3]Key Laboratory of Molecular Imaging, Chinese Academy of Sciences, Beijing, China.

[4]University of Chinese Academy of Sciences, Beijing, China.

[5]Department of General Surgery, Sun Yat-Sen Memorial Hospital, Sun Yat-Sen University, Guangzhou, China.

WEB
This is a web exclusive article.

Supplemental Data
Available online at www.ajronline.org.

AJR 2019; 213:W17–W25

0361–803X/19/2131–W17

OBJECTIVE. The purpose of this study was to investigate the performance of quantitative parameters derived from dual-energy CT (DECT) in the preoperative diagnosis of regional metastatic lymph nodes (LNs) in patients with colorectal cancer.

SUBJECTS AND METHODS. Triphasic contrast-enhanced DECT was performed for 178 patients with colon or high rectal cancer. The morphologic criteria, short-axis diameter, and quantitative DECT parameters of the largest regional LN were measured and compared between pathologically metastatic and nonmetastatic LNs. Univariate and multivariable logistic regression analyses were used to determine the independent DECT parameters for predicting LN metastasis. Diagnostic performance measures were assessed by ROC curve analysis and compared by McNemar test.

RESULTS. A total of 178 largest LNs (72 metastatic, 106 nonmetastatic) were identified in 178 patients. The best single DECT parameter for differentiation between metastatic and nonmetastatic LNs was normalized effective atomic number (Z_{eff}) in the portal venous phase (AUC, 0.871; accuracy, 84.8%). These values were higher than those of morphologic criteria (AUC, 0.505–0.624; accuracy, 47.8–62.4%) and short-axis diameter (AUC, 0.647; accuracy, 66.3%) ($p < 0.05$). The diagnostic accuracy of combined normalized iodine concentration in the arterial phase and normalized effective atomic number in the portal venous phase was further improved to 87.1% (AUC, 0.916).

CONCLUSION. Quantitative parameters derived from DECT can be used to improve preoperative diagnostic accuracy in evaluation for regional metastatic LNs in patients with colorectal cancer.

Colorectal cancer (CRC) is the third most prevalent cancer and ranks as the second leading cause of cancer-related deaths globally [1]. Accurate preoperative diagnosis of lymph node (LN) metastasis is an important determinant of tumor stage. It not only informs prognosis but also is essential for treatment decisions for patients with CRC [2, 3]. For example, patients with stage III disease who have metastatic regional LNs can be treated with chemotherapy to downstage disease before surgery and to decrease the risk of local recurrence after resection [4, 5]. The Fluoropyrimidine, Oxaliplatin, and Targeted Receptor Preoperative Therapy (FOxTROT) trial was initiated to evaluate whether neoadjuvant chemotherapy can improve long-term outcome among patients with operable high-risk colon cancer [6]. Although imaging studies, such as endoluminal sonography, CT, MRI, and PET, are promising for assessing the depth of cancer invasion (T category), their diagnostic accuracies for LN metastasis vary from 54% to 80% [7–12]. Accurate preoperative identification of LN metastasis remains highly challenging [7, 10, 13].

CT is commonly included in the preoperative workup of patients with CRC because it is a quick one-stop examination of the chest and abdomen for local and distant staging [8, 14]. With the introduction of material characterization and decomposition functions, dual-energy CT (DECT) has been found promising for improving diagnostic accuracy for differentiation between malignant and benign tumors [15] and for differentiating metastatic LNs from nonmetastatic LNs, as in papillary thyroid cancer and gastric cancer [16–18]. However, there are limited data on DECT of LNs in CRC. Only two small cohort studies have shown that DECT parameters can be used to differentiate metastatic from nonmetastatic LNs in patients with

CRC [13, 19]. The diagnostic performance of DECT for preoperative LN metastasis remains to be evaluated in a large cohort of patients with CRC.

In this study, DECT was prospectively performed in a large cohort of patients with CRC, and quantitative DECT parameters of regional lymph nodes were derived. The purpose of this study was to assess the performance of DECT parameters in the preoperative diagnosis of regional LN metastasis in patients with CRC.

Subjects and Methods

Patients

This prospective single-center study received institutional ethics committee approval. Written informed consent was obtained from all subjects. Patients with CRC were consecutively enrolled from May 2015 to May 2017. Patients were eligible for enrollment if they had endoscopic biopsy–proven colon or rectal cancer and had an order for chest and abdominal CT. Patients were excluded for the following reasons: previous radiotherapy, chemotherapy, or chemoradiotherapy; no surgical resection of tumor owing to advanced disease (stage IV, according to the TNM [20, 21]); no target LNs or measurable LNs at CT (short-axis diameter < 3 mm); middle or low rectal cancer; contraindications to administration of iodine-based contrast or CT (e.g., pregnancy or metallic implant in the pelvis); and inability to provide informed consent. Two hundred thirty-five patients were enrolled in this study. Fifty-seven patients were excluded because they had middle or low rectal cancer (n = 24), had no target LN or measurable LNs (n = 21), or did not undergo surgical resection (n = 12). Finally, 178 patients were included in the analysis (Fig. 1). The clinicopathologic characteristics of the 178 patients are summarized in Table 1.

TABLE 1: Clinicopathologic Characteristics of 178 Patients With Colorectal Cancer

Characteristic	Metastatic Lymph Nodes (n = 72)	Nonmetastatic Lymph Nodes (n = 106)	p
Age (y)	55.38 ± 13.42	57.09 ± 12.32	0.382[a]
Sex			0.057[b]
Male	45 (62.50)	74 (69.81)	
Female	27 (37.50)	32 (30.19)	
Primary site			0.518[b]
Right hemicolon	23 (31.94)	18 (16.98)	
Left hemicolon	1 (1.39)	5 (4.72)	
Sigmoid colon	19 (26.39)	46 (43.40)	
High rectum	29 (40.28)	37 (34.90)	
Carcinoembryonic antigen level			0.042[b]
Normal	17 (23.61)	59 (55.66)	
Abnormal	55 (76.39)	47 (44.34)	
Histologic grade			0.119[b]
Well differentiated	10 (13.89)	22 (20.75)	
Moderately differentiated	59 (81.94)	84 (79.25)	
Poorly differentiated	3 (4.17)	0 (0.00)	
pTNM category			0.048[b]
T1	0 (0.00)	1 (0.94)	
T2	2 (2.78)	10 (9.43)	
T3	24 (33.33)	41 (38.68)	
T4	46 (63.89)	54 (50.94)	

Note—Except for age, which is mean ± SD, values are number with percentages in parentheses.
[a] t test.
[b] Fisher exact test.

CT

CT was performed with a spectral 64-MDCT system (Discovery CT750 HD, GE Healthcare). Each patient received orally administered colon-cleansing preparation (polyethylene glycol electrolyte solution) 12 hours before the CT examination and were instructed to drink 1000 mL of isotonic solution (2.5% mannitol solution) 1 hour before the CT examination. All scanning was performed in the craniocaudal direction with the patient supine. The whole abdomen was scanned from the dome of the right diaphragm to the anal verge. Unenhanced scanning was performed in the conventional helical mode at a tube voltage of 120 kVp and tube current of 350 mA during a full-inspiratory breath-hold. Then, an IV injection of a nonionic iodinated contrast medium (Iohexol 350 mg I/dL, GE Healthcare) was administered at a dose of 1.5 mL/kg through a dual-head injector at a flow rate of 4 mL/s followed by a bolus injection of 50 mL saline solution given at the same flow rate.

Triphasic contrast-enhanced CT images were obtained in dual-energy rapid tube voltage switching mode (80–140 kVp) by means of the gemstone imaging protocol at preset 54 and a tube current of 375 mA. To discriminate cirrhotic nodules from liver metastases, triphasic contrast-enhanced CT of the abdomen and pelvis is a routine part of the preoperative workup of patients with CRC at our institution owing to the high prevalence of covert hepatis virus B–related cirrhosis. The scanning delay for hepatic arterial phase (HAP) imaging was determined with automated scan triggering software (SmartPrep, GE Healthcare). Arterial phase scanning automatically began 7.6 seconds after the trigger attenuation threshold (100 HU) was reached at the level of the descending aorta. At a delay of 18 seconds after the arterial phase, portal venous phase (PVP) scanning was performed. Equilibrium phase scanning was performed with a delay of 45 seconds after the PVP.

Other acquisition parameters were as follows: collimation thickness, 64 × 0.625 mm; rotation speed, 0.6 second; helical pitch, 0.984. All CT raw data were reconstructed into contiguous axial images with a section thickness of 1.25 mm and an increment of 1 mm, an FOV of 35 cm, and a matrix of 512 × 512. Unenhanced CT data were reconstructed by use of a standard reconstruction algorithm. The contrast-enhanced CT data were reconstructed by use of 50% adaptive statistical iterative reconstruction (ASiR, GE Healthcare) blending and transferred to an advanced workstation (AW 4.6, GE Healthcare) for analysis.

Imaging Analysis

The DECT datasets were analyzed with the viewer software at the workstation. Three subgroups of image datasets—polychromatic images corresponding to conventional 120-kVp imaging, monochromatic images with photon energies ranging from 40 to 140 keV, and iodine-based material decomposition images—were reconstructed. First, the largest regional LN was identified by a radiologist (10 years of experience with CT diag-

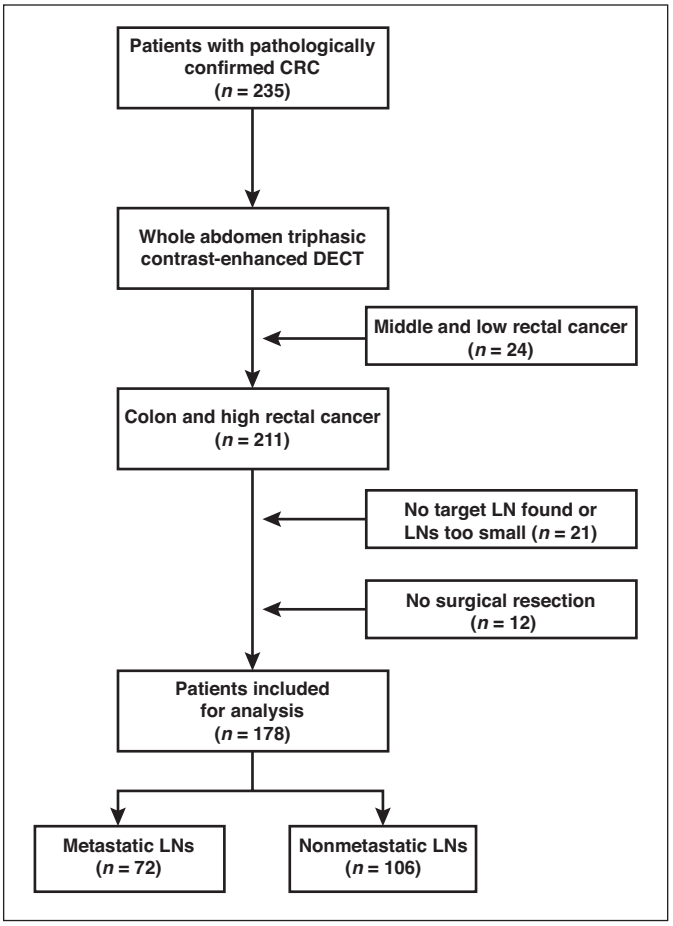

Fig. 1—Flowchart shows overview of patient inclusion and exclusion. CRC = colorectal cancer, DECT = dual-energy CT, LN = lymph node.

nosis) and a general surgeon (10 years of experience in gastrointestinal surgery involved to ensure correct labeling of the largest LNs during surgery) in consensus on 70-keV monochromatic PVP images on which visualization of LNs was optimal because of the best contrast-to-noise ratio.

The regional LNs included peritumoral mesenteric LNs around the superior mesenteric artery (right hemicolon), inferior mesenteric artery (left hemicolon, sigmoid colon, and high rectum), and root of the mesentery. The short- and long-axis diameters of all LNs visible in these regions were measured, and the largest LN was identified. The short-axis diameter of the largest LN was measured by the radiologist using multiplanar reformation. The morphologic features of visible LNs were subjectively assessed on the conventional 120-kVp PVP images. The morphologic criteria for metastatic LNs were as follows: round shape (short-to-long axis diameter ratio > 0.8), internal heterogeneity, irregular outer border, contrast enhancement (attenuation > 100 HU), and cluster of three or more normal-sized lymph nodes, as previously described [22].

Quantitative DECT parameters were independently measured by two radiologists (20 and 10 years of experience). They manually drew a free-hand ROI on the transverse slice showing the maximal dimension of the largest LN. The ROI outline was made as large as possible (mean area, 30.4 mm^2; range, 9.7–95.3 mm^2) to cover the entire LN (Figs. 2A and 3A) with care to exclude the surrounding fat and vessels. At the same time, an oval ROI (mean area, 125.8 mm^2; range, 80.4–186.8 mm^2) was placed on the descending aorta at the level of the right renal artery. The DECT parameters iodine concentration (IC) in milligrams per cubic centimeter and normalized effective atomic number (Z_{eff}) were obtained. The IC and Z_{eff} of the LN were normalized to those of the aorta to derive normalized IC (NIC) and normalized Z_{eff} according to the following formulas: $NIC = IC_{LN} / IC_{aorta}$ and normalized $Z_{eff} = Z_{eff\ LN} / Z_{eff\ aorta}$. The slope of the attenuation curve (λ) was calculated as the difference between the CT value at 40 keV and that at 70 keV divided by the energy difference (30 keV) [17]. For each patient, the NIC, normalized Z_{eff}, and slope of the attenuation curve of the same largest lymph node were measured on all triphase contrast-enhanced images. To ensure consistency between the measurements, the triphase images were simultaneously loaded into the workstation, and the size, shape, and position of the ROIs in three phases were kept the same by use of the copy and paste functions. Measurements by two radiologists were averaged to produce the final values for analysis.

Surgical Resection and Pathologic Examination

Surgical resection of the CRC was performed within 7 days after DECT. The surgeon who had previously identified the largest LNs on CT images carefully labeled the same largest LNs during surgery. For intraoperative identification, LN size, distance between the tumor and anatomic landmarks such as the superior and inferior mesenteric arteries, and the position and distance from the primary lesion were used for reference [23]. The entire resected colorectal specimens were processed for conventional histologic examination. The pathologist confirmed the presence of the labeled largest LNs. The results of histologic analysis of the primary tumor and all regional LNs were recorded.

Statistical Analysis

Quantitative variables were expressed as the mean ± SD. The interclass correlation coefficient (ICC) was used to evaluate interobserver agreement between two radiologists for the measurements of DECT parameters. An independent two-sample *t* test was performed to compare the differences in short-axis diameter, NIC, normalized Z_{eff}, and slope of the attenuation curve between metastatic and nonmetastatic LNs. Univariable logistic regression analysis was used to determine whether a single parameter could be used to differentiate between metastatic and nonmetastatic LNs.

The significant parameters were further analyzed with the least absolute shrinkage and selection operator (LASSO) logistic regression model to select the most useful predictive factors by shrinking the coefficients toward zero by setting a constraint on the sum of the absolute standardized coefficients [14]. Multivariable logistic regression analysis of variables selected in the LASSO regression model was performed to determine the independent parameters for predicting the presence of metastatic LNs. ROC curves were used to determine the diagnostic utility of morphologic criteria, short-axis diameter, and quantitative DECT parameters. ROC AUC, sensitivity, specificity, positive predictive value, negative predictive value, and accuracy were calculated and compared by McNemar test. The optimal threshold was determined with the maximum Youden index. Net reclassification improvement and integrated discrimination improvement were applied to detect the improved discriminatory effects of DECT parameters [24]. LASSO logistic regression and ROC analyses were performed with the glmnet,

pROC, survival, nircens, and ggplot2 packages of R software (version 3.5.0, R Project). Other statistical analyses were performed with SPSS software (version 20.0, IBM SPSS). A value of $p < 0.05$ indicated a statistically significant difference.

Results

Quantitative Parameters

A total of 178 largest LNs were identified in 178 patients. Among them, 72 were metastatic and 106 were nonmetastatic. The short-axis diameter and DECT measurements are shown in Table 2. The ICC analysis indicated good concordance between interobserver measurements (ICC, 0.839–0.944). The short-axis diameter of metastatic LNs was significantly greater than that of nonmetastatic LNs ($p < 0.05$). All DECT parameters were significantly lower in metastatic LNs than in nonmetastatic LNs ($p < 0.05$) (Table 2 and Figs. 2B–2D and 3B–3D). Univariate binary logistic regression analysis showed that metastatic and nonmetastatic LNs could be differentiated with each DECT parameter ($p < 0.05$). These nine parameters were reduced to two potential independent predictors—HAP NIC and PVP normalized Z_{eff}—in LASSO logistic regression analysis with 10-fold cross-validation ($\lambda = 0.2282$). Further multivariate logistic regression analysis showed that HAP NIC and normalized PVP Z_{eff} were independent predictors ($p < 0.05$). The regression equation was as follows: logit $p_{mLN} = -43.944 + 25.111$ NIC HAP + 45.166 normalized PVP Z_{eff}, where logit p_{mLN} is the probability that an LN is metastatic.

Diagnostic Performance

ROC curve analyses of the morphologic criteria, short-axis diameter, and each DECT parameter are shown in Tables 3 and 4 and Figure 4. The AUC of short-axis diameter was 0.647 with accuracy of 66.3% at the optimal threshold of 8.250 mm. The best single DECT parameter was normalized PVP Z_{eff} with an AUC of 0.871 and accuracy of 84.8% at the optimal threshold of 0.881, which were higher than those of morphologic criteria (AUC, 0.505–0.624; accuracy, 47.8–62.4%) and short-axis diameter ($p < 0.05$). At the optimal predictive probability threshold of 0.366, the AUC of combined HAP NIC and normalized PVP Z_{eff} was 0.916; sensitivity, 83.3%; specificity, 89.6%; positive predictive value, 84.5%; negative predictive value, 88.8%; and accuracy, 87.1% (Table 4 and Fig. 4).

The diagnostic accuracy of combined HAP NIC and normalized PVP Z_{eff} was significantly greater than that of normalized PVP Z_{eff} or short-axis diameter individually ($p < 0.05$).

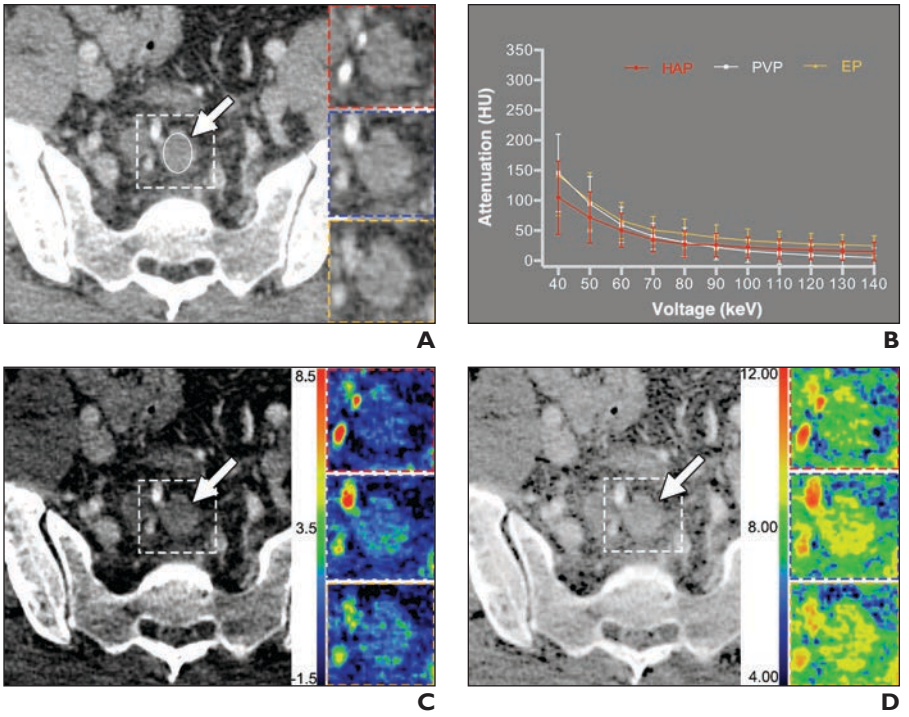

Fig. 2—42-year-old man with poorly differentiated pathologic T3N2 rectal adenocarcinoma. Representative dual-energy CT examination of metastatic lymph node. Dashed line indicates location of inserts. Inserts show hepatic arterial phase (*red*), portal venous phase (*blue*), and equilibrium phase (*yellow*) images.
A, Portal venous phase 70-keV monochromatic contrast-enhanced CT images show largest metastatic lymph node (*arrow*) around superior rectal artery with short-axis diameter of 12.1 mm. ROI (*oval*) was drawn to cover entire lymph node; area is 59.2 mm^2.
B, Graph shows spectral attenuation curves of metastatic lymph node. Slopes of attenuation curves are 1.70 in hepatic arterial phase (HAP), 3.36 in portal venous phase (PVP), and 3.15 in equilibrium phase (EP).
C, Portal venous phase contrast-enhanced iodine-based material decomposition CT images show iodine concentrations are 0.81 ± 0.72 mg/cm^3 in hepatic arterial phase, 1.70 ± 0.67 mg/cm^3 in portal venous phase, and 1.58 ± 0.75 mg/cm^3 in equilibrium phase. Arrow indicates largest metastatic lymph node.
D, Portal venous phase contrast-enhanced effective atomic number CT images show effective atomic numbers are 8.08 ± 0.45 in hepatic arterial phase, 8.61 ± 0.36 in portal venous phase, and 8.54 ± 0.43 in equilibrium phase. Arrow indicates largest metastatic lymph node.

Further net reclassification improvement and integrated discrimination improvement showed reclassification was significantly increased in the combination of HAP NIC and normalized PVP Z_{eff} compared with short-axis diameter (Table S1) (net reclassification improvement, 0.478; integrated discrimination improvement, 0.457; $p < 0.001$). (Table S1 can be viewed in the *AJR* electronic supplement to this article at www.ajronline.org.) Moreover, 31 LNs had a short-axis diameter smaller than 5 mm, 124 LNs had a short-axis diameter of 5–10 mm, and 23 LNs had a short-axis diameter greater than 10 mm. The diagnostic accuracy of combined HAP NIC and normalized PVP Z_{eff} was 83.9% for LNs smaller than 5 mm, 87.1% for LNs measuring 5–10 mm, and 91.3% for LNs larger than 10 mm.

Discussion

Our study showed that quantitative DECT parameters, especially HAP NIC and normalized PVP $Z_{eff,}$ had greater diagnostic utility in the preoperative identification of LN metastasis in patients with CRC than did conventional morphologic and size criteria. When combined, HAP NIC and normalized PVP Z_{eff} further improved diagnostic accuracy for metastatic LNs.

Single-energy CT has good sensitivity for preoperative T categorization of CRC, and the use of CT colonography can increase its accuracy [25]. Compared with CT, MRI has lower sensitivity and comparable specificity for T categorization overall [26]. A recent comparative study showed that the diagnostic performance of MRI may be better than that of MDCT for T categorization of high-risk stage II and III colon cancers.

In particular, use of MRI reduced the false-positive rate [27]. For N categorization, MRI has moderate diagnostic sensitivity and specificity [28]. Its diagnostic performance is comparable to that of CT [25].

TABLE 2: Quantitative Dual-Energy CT Characteristics of Metastatic and Nonmetastatic Lymph Nodes

Characteristic	Colon and High Rectal Cancer (n = 178)			
	Metastatic Lymph Nodes (n = 72)	Nonmetastatic Lymph Nodes (n = 106)	t	p
Short-axis diameter (mm)	8.20 ± 3.15	6.63 ± 1.94	4.134	< 0.001
Normalized iodine concentration (mg/cm^3)				
Hepatic arterial phase	0.13 ± 0.05	0.20 ± 0.05	–9.147	< 0.001
Portal venous phase	0.39 ± 0.14	0.56 ± 0.10	–9.053	< 0.001
Equilibrium phase	0.55 ± 0.17	0.64 ± 0.15	–3.991	< 0.001
Normalized effective atomic number				
Hepatic arterial phase	0.71 ± 0.03	0.74 ± 0.04	–5.519	< 0.001
Portal venous phase	0.86 ± 0.04	0.91 ± 0.02	–10.339	< 0.001
Equilibrium phase	0.91 ± 0.04	0.93 ± 0.03	–4.225	< 0.001
Slope of attenuation curve				
Hepatic arterial phase	3.13 ± 1.20	4.70 ± 1.20	–8.536	< 0.001
Portal venous phase	4.61 ± 2.00	5.86 ± 1.29	–5.072	< 0.001
Equilibrium phase	4.53 ± 1.68	5.13 ± 1.22	–2.743	0.007

Note—Values are mean ± SD.

A variety of diagnostic standards, such as size, border, degree and pattern of enhancement, necrosis, extranodal extension, signal intensity, and apparent diffusion coefficient, have been used to assess the status of LNs in patients with CRC. The preoperative prediction of LN involvement still relies mainly on size criteria in daily clinical practice [13, 17], and the commonly used size criteria are any node larger than 1 cm or a cluster of three or more nodes smaller than 1 cm [7–9]. A meta-analysis of 19 studies showed that the pooled sensitivity and specificity of size criteria in single-energy CT were 70% and 78% [7], which was comparable to those of MRI [10]. Among various types of single-energy CT scanners, MDCT has the highest sensitivity compared with conventional and single-detector helical CT (77% vs 68% and 64%) but also the lowest specificity (38%, 63%, and 69%) [25].

The diagnostic performance of CT colonography for detecting malignant nodes was also limited, both sensitivity and specificity being less than 70% [26]. In our study, the diagnostic accuracy of short-axis diameter was moderate (66.3%) at a threshold of 8.250 mm. This finding is similar to a previously reported overall accuracy of 65.7% for short-axis diameter at a threshold of 5.45 mm [13]. Except for moderate diagnostic accuracy, morphologic criteria may be less reliable among different observers [13]. In our study, the diagnostic accuracy of morphologic criteria was 47.8–61.2%. The combined morphologic criteria had higher sensitivity (97.2%) but lower specificity (14.2%), which is consistent with a previous report [22]. However, there is also no worldwide consensus on morphologic criteria in terms of measuring method (short or long axis), size, shape, or enhancement pattern [16]. Moreover, morphologic criteria also appear to have intrinsic limitations in LNs smaller than 5 mm in diameter [23].

DECT allows differentiation of materials with different molecular compositions based on their attenuation profiles [13, 19]. DECT can be used to discriminate between materials (calcium, iodine, water, fat) it entails two-material decomposition technique [18, 29], and IC can be measured on iodine-water images to reflect enhancement of lesions [18, 30]. Pathophysiologic changes that affect tissue blood volume and vessel permeability will be reflected in the magnitude of iodine content [31–34], which can be detected with characteristic parameters from contrast-enhanced DECT [13, 19, 35, 36], such as IC, Z_{eff}, and slope of the attenuation curve [37]. These quantitative parameters have been found to improve tumor detection and diagnostic accuracy [15]. A 2015 study of 55 patients with rectal cancers showed that the diagnostic accuracy of HAP NIC for metastatic LNs was 61.0% and that of PVP NIC was 72.4% [13].

In a retrospective study of 28 patients with CRC, PVP IC was found to have the greatest utility for discriminating LN metastases with an accuracy of 87.9% [19]. In our study, triphase contrast-enhanced DECT was performed for a large cohort of patients with CRC. Our results showed that NIC, normalized PVP Z_{eff}, and slope of the attenuation curve in the HAP, PVP, and equilibrium phase were better than short-axis diameter for differentiation between metastatic and nonmetastatic LNs. The best single DECT parameter for discriminating metastatic LNs, however, was normalized PVP Z_{eff} with an accuracy of 84.8%, which is obviously greater than that of the size criteria. Radiologic-pathologic correlation per LN is indispensable for identifying metastatic LNs. However, it is challenging to connect LNs on CT images to their corresponding excised specimens in patients with CRC [13, 16]. Thus, the precise count of lymph nodes poses a considerable challenge.

Different radiologic-pathologic one-to-one comparison methods have been used to determine the diagnostic performance of DECT for metastatic LNs in patients with CRC [13, 19]. One strategy is that regional LNs were categorized into four regional groups: peritumoral, perirectal, pericolic, and inferior mesenteric artery. If all of the harvested LNs were metastatic in each group, then all of the identified LNs on the CT images were considered metastatic LNs in the corresponding group. The same parameters were applied to the nonmetastatic LNs. Another method is to measure DECT parameters in the three largest LNs for patients with pN0 nodes; otherwise, the parameters are measured in pathologic metastatic LNs next to the primary tumor or those with obvious heterogeneous enhancement or a speculated appearance for analysis [19].

Unlike the investigators in the two earlier studies [13, 19], we selected the largest regional LN in each patient for analysis. This method can achieve complete node-by-node radiologic-pathologic correlation, although the largest LN might not definitely represent the metastatic LN in all patients. The number of LNs might have increases if more than one node in each patient had been evaluated. However, a study of rectal cancer specimens imaged with DECT [35] showed that the exact number of LNs on preoperative CT images cannot be compared with

TABLE 3: Results of ROC Analysis of Morphologic Criteria in Differential Diagnosis of Metastatic and Nonmetastatic Lymph Nodes

Feature	AUC	Sensitivity (%)	Specificity (%)	Positive Predictive Value (%)	Negative Predictive Value (%)	Accuracy (%)
Round shape	0.621 (0.549–0.694)	66.7 (54.5–77.1)	66.7 (54.5–77.1)	51.6 (41.1–62.0)	71.8 (60.8–80.7)	61.2 (53.7–68.4)
Internal heterogeneity	0.624 (0.551–0.697)	62.5 (50.2–73.4)	62.3 (52.3–71.3)	52.9 (41.9–63.7)	71.0 (60.5–79.7)	62.4 (54.8–69.5)
Irregular outer border	0.602 (0.529–0.676)	63.9 (51.6–74.6)	56.6 (46.6–66.1)	50.0 (39.5–60.5)	69.8 (58.8–79.0)	59.6 (52.0–66.8)
Contrast enhancement	0.505 (0.444–0.566)	20.8 (12.5–32.3)	80.2 (71.1–87.0)	41.7 (26.0–59.1)	59.8 (51.3–67.9)	56.2 (48.6–63.6)
Cluster	0.537 (0.469–0.605)	31.9 (21.7–44.1)	41.7 (26.0–59.1)	46.9 (32.8–61.6)	62.0 (53.0–70.3)	57.9 (50.2–65.2)
Combined	0.557 (0.518–0.595)	97.2 (89.4–99.5)	14.2 (8.4–22.6)	43.5 (35.8–51.5)	88.2 (62.2–97.9)	47.8 (40.2–55.4)

Note—Data in parentheses are 95% CIs. Round shape indicates a short-to-long axis diameter ratio > 0.8; contrast enhancement, attenuation > 100 HU; cluster, a cluster of three or more normal-sized lymph nodes; combined, combination of round shape, internal heterogeneity, irregular outer border, contrast enhancement, and cluster.

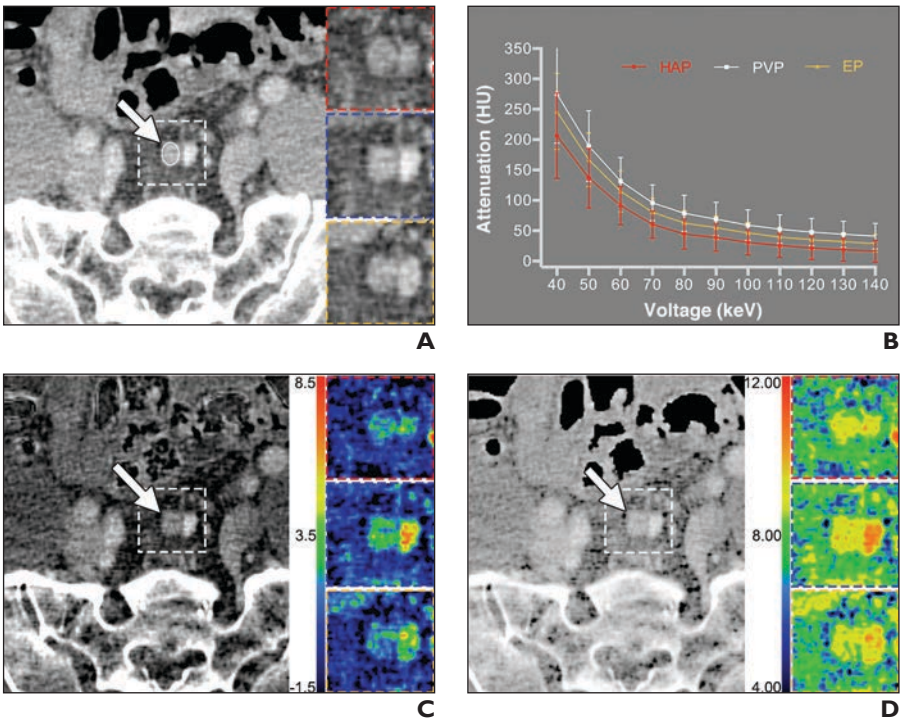

Fig. 3—63-year-old man with moderately differentiated pathologic T2N0 rectal adenocarcinoma. Representative dual-energy CT examination of nonmetastatic lymph node. Dashed line indicates location of inserts. Inserts show hepatic arterial phase (*red*), portal venous phase (*blue*), and equilibrium phase (*yellow*) images.

A, Portal venous phase 70-keV monochromatic contrast-enhanced CT images show largest, metastatic lymph node (*arrow*) around superior rectal artery with short-axis diameter of 6.7 mm. ROI (*oval*) was drawn to cover entire lymph node; area is 23.6 mm^2.

B, Graph shows spectral attenuation curves of nonmetastatic lymph node. Slopes of attenuation curves are 4.86 in hepatic arterial phase (HAP), 5.97 in portal venous phase (PVP), and 5.53 in equilibrium phase (EP).

C, Portal venous phase contrast-enhanced iodine-based material decomposition CT image shows iodine concentrations are 2.45 ± 0.77 mg/cm^3 in hepatic arterial phase, 3.02 ± 0.81 mg/cm^3 in portal venous phase, and 2.81 ± 0.67 mg/cm^3 in equilibrium phase. Arrow indicates largest metastatic lymph node.

D, Portal venous phase contrast-enhanced effective atomic number CT images show effective atomic numbers are 9.02 ± 0.37 in hepatic arterial phase, 9.26 ± 0.36 in portal venous phase, and 9.18 ± 0.30 in equilibrium phase. Arrow indicates largest metastatic lymph node.

the specimen images because of the larger number of visible lymph nodes on specimen images. This would also cause dependency problems regarding the influence of multiple nodes per patient [18]. Taken together, the radiologic-pathologic one-to-one matching per LN in our study would be more preferable for determining the diagnostic performance of DECT parameters and their cutoff values for metastatic LNs in patients with CRC.

In our study, nine DECT parameters differed between metastatic and nonmetastatic LNs, and most of them had greater diagnostic utility than the size criteria. These nine parameters were reduced to two independent predictors: HAP NIC and normalized PVP Z_{eff}. The combination of HAP NIC and normalized PVP Z_{eff} had diagnostic accuracy of 87.1%, which is higher than the accuracy of the size criterion (66.3%). It has been reported that the pooled diagnostic accuracy of PET and PET/CT for preoperative N status is 70.0–72.4% [11, 12] and that radiomic features based on conventional PVP CT images have good accuracy for preoperative prediction of lymph node metastasis (C-index, 0.778) [14].

In our study, a quantitative DECT parameter, normalized PVP Z_{eff}, had sensitivity of 73.6% and specificity of 92.4% for detecting metastatic LNs. These values are higher than their counterparts for single-energy CT [25] and CT colonography [26]. Compared with these modalities, quantitative DECT has favorable performance for preoperative prediction that an LN is metastatic. In addition, quantitative DECT parameters can be easily derived because they do not require a complicated calculation of high-dimensional image data. Moreover, DECT can provide both anatomic and functional information in a single contrast-enhanced CT examination. Notably, combined HAP NIC and normalized PVP Z_{eff} had a positive predictive value of 84.5% for metastatic LNs in patients with CRC in our study. Neoadjuvant treatment strategies for patients with colon cancer that improve compliance and have potential for downstaging of disease before surgical treatment are being developed [7].

Preliminary results of the FOxTROT trial showed that patients with radiologically staged, locally advanced operable primary

TABLE 4: Results of ROC Analysis of Short-Axis Diameter and Quantitative Dual-Energy CT Parameters in Differential Diagnosis of Metastatic and Nonmetastatic Lymph Nodes

Parameter	Threshold	AUC	Sensitivity (%)	Specificity (%)	Positive Predictive Value (%)	Negative Predictive Value (%)	Accuracy (%)
Short-axis diameter (mm)	8.250	0.647 (0.564–0.731)	43.1 (31.6–55.2)	82.1 (73.2–88.6)	62.0 (47.2–75.0)	67.8 (59.0–77.8)	66.3 (58.8–73.2)
Normalized iodine concentration							
Hepatic arterial phase	0.177	0.839 (0.781–0.898)	87.5 (77.1–93.8)	66.0 (56.1–74.8)	63.6 (53.3–72.9)	88.6 (79.0–94.3)	74.7 (67.7–80.9)
Portal venous phase	0.500	0.840 (0.776–0.903)	83.3 (72.3–90.7)	72.6 (63.0–80.6)	67.4 (56.6–76.8)	86.5 (77.2–92.5)	77.0 (70.1–82.9)
Equilibrium phase	0.538	0.662 (0.579–0.745)	54.2 (42.1–65.8)	77.4 (68.0–84.7)	61.9 (48.8–73.6)	71.3 (62.0–79.2)	68.0 (60.6–74.8)
Normalized effective atomic number							
Hepatic arterial phase	0.716	0.727 (0.652–0.803)	62.5 (50.2–73.4)	77.4 (68.0–84.7)	65.2 (52.7–76.0)	75.2 (65.9–82.8)	71.9 (64.7–78.4)
Portal venous phase	0.881	0.871 (0.811–0.930)	73.6 (61.7–83.0)	92.4 (85.2–96.4)	86.9 (75.2–93.8)	83.7 (75.5–89.7)	84.8 (78.7–89.8)
Equilibrium phase	0.920	0.672 (0.590–0.754)	61.1 (48.9–72.2)	69.8 (60.0–78.1)	57.9 (46.0–69.0)	72.5 (62.7–80.7)	66.3 (58.8–73.2)
Slope of attenuation curve							
Hepatic arterial phase	3.685	0.827 (0.764–0.890)	72.2 (60.2–81.8)	84.0 (75.2–90.1)	75.4 (63.3–84.6)	81.6 (72.8–88.2)	79.2 (72.5–84.9)
Portal venous phase	4.984	0.737 (0.657–0.818)	68.0 (56.0–78.3)	76.4 (67.0–83.9)	66.2 (54.2–76.5)	77.9 (68.5–85.2)	73.0 (65.9–79.4)
Equilibrium phase	3.860	0.616 (0.527–0.705)	41.7 (30.4–53.9)	85.8 (77.4–91.6)	66.7 (50.9–79.6)	68.4 (59.7–76.0)	68.0 (60.6–74.8)
Combined[a]	0.366	0.916 (0.873–0.960)	83.3 (72.3–90.7)	89.6 (81.8–94.4)	84.5 (73.5–91.6)	88.8 (80.9–93.8)	87.1 (81.2–91.6)

Note—Data in parentheses are 95% CIs.
[a]Combination of normalized iodine concentration in hepatic arterial phase and normalized effective atomic number in portal venous phase.

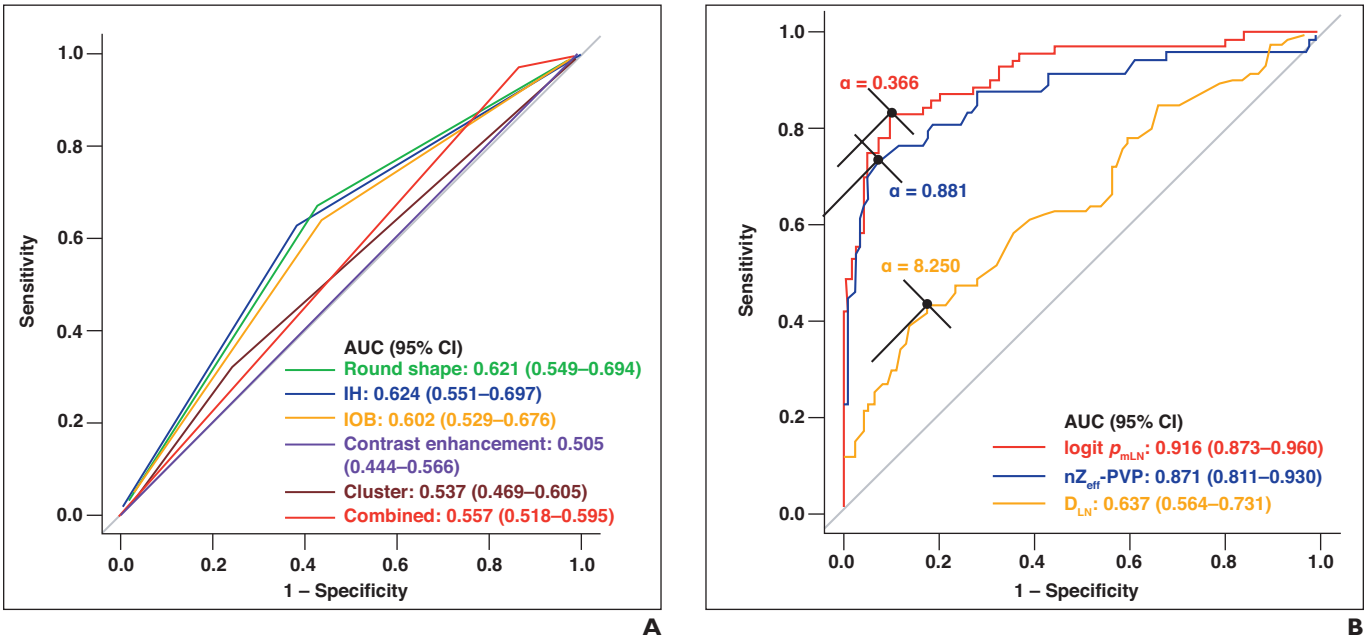

Fig. 4—ROC analysis.
A, Graph shows ROC curves of each morphologic feature for differentiating metastatic and nonmetastatic lymph nodes in patients with colorectal cancer. "Round shape" indicates short-to-long axis diameter ratio > 0.8; IH, internal heterogeneity; IOB, irregular outer border; contrast enhancement, attenuation > 100 HU; cluster, cluster of three or more normal-sized lymph nodes; combined, combined morphologic criteria.
B, Graph shows ROC curves for combined normalized iodine concentration in hepatic arterial phase and normalized effective atomic number in portal venous phase (logit p_{mLN}, which indicates probability that metastatic lymph node [LN] is present); single parameter of normalized effective atomic number in portal venous phase (nZ_{eff}-PVP); and short-axis diameter of lymph nodes (D_{LN}) for differentiating metastatic and nonmetastatic lymph nodes in patients with colorectal cancer. α = threshold (*black*).

colon cancer can benefit from neoadjuvant chemotherapy with resultant lower tumor stages, fewer positive lymph nodes, and fewer positive resection margins [6]. CT colonography has been found feasible for preoperative local staging of higher-risk colon cancers for which neoadjuvant chemotherapy is more suitable on the basis of the FOxTROT trial criteria [26]. These findings suggest that many patients would have been treated with neoadjuvant chemotherapy if the diagnosis of metastatic LNs had been made according to preoperative DECT quantitative parameters. As such, these patients would benefit from the better planning of optimal therapy. Of note is that a single DECT parameter, normalized PVP Z_{eff}, had high diagnostic accuracy (84.8%) for the detection of regional LN metastasis. When PVP Z_{eff} was combined with HAP NIC, the diagnostic accuracy further increased to 87.1%. These results suggest that PVP and HAP imaging data both are useful for detecting metastatic LNs by use of DECT parameters. In addition, a complete preoperative evaluation of patients with colon cancer includes not only staging of the primary tumor but also CT evaluation of distant metastases in the liver [22]. Thus, a multiphase scanning protocol is still needed for preoperative DECT of patients with CRC.

There were several limitations to our study. First, unlike in a previous study [22], in our study mesenteric LNs were not divided into three regions according to their anatomic distribution. Only radiologically-pathologically matched LNs were included for assessment of DECT parameters. Further studies are needed to test the performance of DECT parameters in the preoperative diagnosis of LN metastasis in different mesenteric regions. Second, because our study focused on the N status of CRC, T and M status were not assessed at DECT. Previous studies have already shown that CT has good diagnostic accuracy for T categorization of colon cancers [6, 10, 25]. In particular, preoperative staging CT is accurate for differentiating tumors confined to the bowel wall from those invading beyond the muscularis propria [7–12].

Conclusion

Our study results showed that multiple DECT parameters can be used to differentiate metastatic from nonmetastatic LNs in patients with CRC. Most of the DECT parameters have higher diagnostic accuracy than the conventional size criteria. Combined assessment of HAP NIC and normalized PVP Z_{eff} can increase preoperative diagnostic accuracy in evaluation for metastatic LNs.

References

1. Bray F, Ferlay J, Soerjomataram I, Siegel RL, Torre LA, Jemal A. Global cancer statistics 2018: GLOBOCAN estimates of incidence and mortality worldwide for 36 cancers in 185 countries. *CA Cancer J Clin* 2018; 68:394–424
2. Bilchik A, Nissan A, Wainberg Z, et al. Surgical quality and nodal ultrastaging is associated with long-term disease-free survival in early colorectal cancer: an analysis of 2 international multicenter prospective trials. *Ann Surg* 2010; 252:467–474; discussion, 474–466
3. Oltedal S, Gilje B, Kørner H, et al. Detection of occult metastases in sentinel lymph nodes from colon cancer patients by K-ras mutation peptide nucleic acid clamp PCR. *Ann Surg* 2010; 251:1087–1091
4. GrahAm JS, Cassidy J. Adjuvant therapy in colon cancer. *Expert Rev Anticancer Ther* 2012; 12:99–109
5. Dienstmann R, Salazar R, Tabernero J. Personalizing colon cancer adjuvant therapy: selecting optimal treatments for individual patients. *J Clin Oncol* 2015; 33:1787–1796
6. Foxtrot Collaborative Group. Feasibility of preoperative chemotherapy for locally advanced, operable colon cancer: the pilot phase of a randomised controlled trial. *Lancet Oncol* 2012; 13:1152–1160
7. Dighe S, Purkayastha S, Swift I, et al. Diagnostic precision of CT in local staging of colon cancers: a meta-analysis. *Clin Radiol* 2010; 65:708–719
8. de Vries FE, da Costa DW, van der Mooren K, van Dorp TA, Vrouenraets BC. The value of pre-operative computed tomography scanning for the assessment of lymph node status in patients with colon cancer. *Eur J Surg Oncol* 2014; 40:1777–1781
9. Filippone A, Ambrosini R, Fuschi M, Marinelli T, Genovesi D, Bonomo L. Preoperative T and N staging of colorectal cancer: accuracy of contrast-enhanced multi-detector row CT colonography—initial experience. *Radiology* 2004; 231:83–90
10. Al-Sukhni E, Milot L, Fruitman M, et al. Diagnostic accuracy of MRI for assessment of T category, lymph node metastases, and circumferential resection margin involvement in patients with rectal cancer: a systematic review and meta-analysis. *Ann Surg Oncol* 2012; 19:2212–2223
11. Ye Y, Liu T, Lu L, et al. Pre-operative TNM staging of primary colorectal cancer by (18)F-FDG PET-CT or PET: a meta-analysis including 2283 patients. *Int J Clin Exp Med* 2015; 8:21773–21785
12. Lu YY, Chen JH, Ding HJ, Chien CR, Lin WY, Kao CH. A systematic review and meta-analysis of pretherapeutic lymph node staging of colorectal cancer by ^{18}F-FDG PET or PET/CT. *Nucl Med Commun* 2012; 33:1127–1133
13. Liu H, Yan F, Pan Z, et al. Evaluation of dual energy spectral CT in differentiating metastatic from non-metastatic lymph nodes in rectal cancer: initial experience. *Eur J Radiol* 2015; 84:228–234
14. Huang YQ, Liang CH, He L, et al. Development and validation of a radiomics nomogram for preoperative prediction of lymph node metastasis in colorectal cancer. *J Clin Oncol* 2016; 34:2157–2164
15. Paul J, Vogl TJ, Mbalisike EC. Oncological applications of dual-energy computed tomography imaging. *J Comput Assist Tomogr* 2014; 38:834–842
16. Pan Z, Pang L, Ding B, et al. Gastric cancer staging with dual energy spectral CT imaging. *PLoS One* 2013; 8:e53651
17. Liu X, Ouyang D, Li H, et al. Papillary thyroid cancer: dual-energy spectral CT quantitative parameters for preoperative diagnosis of metastasis to the cervical lymph nodes. *Radiology* 2015; 275:167–176
18. Yang L, Luo D, Li L, et al. Differentiation of malignant cervical lymphadenopathy by dual-energy CT: a preliminary analysis. *Sci Rep* 2016; 6:31020
19. Kato T, Uehara K, Ishigaki S, et al. Clinical significance of dual-energy CT-derived iodine quantification in the diagnosis of metastatic LN in colorectal cancer. *Eur J Surg Oncol* 2015; 41:1464–1470
20. Edge SB, Compton CC. The American Joint Committee on Cancer: the 7th edition of the AJCC cancer staging manual and the future of TNM. *Ann Surg Oncol* 2010; 17:1471–1474
21. Carlson RW, Larsen JK, McClure J, et al. International adaptations of NCCN clinical practice guidelines in oncology. *J Natl Compr Canc Netw* 2014; 12:643–648
22. Rollvén E, Abraham-Nordling M, Holm T, Blomqvist L. Assessment and diagnostic accuracy of lymph node status to predict stage III colon cancer using computed tomography. *Cancer Imaging* 2017; 17:3
23. Cho EY, Kim SH, Yoon JH, et al. Apparent diffusion coefficient for discriminating metastatic from non-metastatic lymph nodes in primary rectal cancer. *Eur J Radiol* 2013; 82:e662–e668
24. Xin J, Chu H, Ben S, et al. Evaluating the effect of multiple genetic risk score models on colorectal cancer risk prediction. *Gene* 2018; 673:174–180
25. Nerad E, Lahaye MJ, Maas M, et al. Diagnostic

accuracy of CT for local staging of colon cancer: a systematic review and meta-analysis. *AJR* 2016; 207:984–995

26. Horvat N, Raj A, Liu S, et al. CT colonography in preoperative staging of colon cancer: evaluation of FOxTROT inclusion criteria for neoadjuvant therapy. *AJR* 2019; 212:94–102
27. Park SY, Cho SH, Lee MA, et al. Diagnostic performance of MRI- versus MDCT-categorized T3cd/T4 for identifying high-risk stage II or stage III colon cancers: a pilot study. *Abdom Radiol (NY)* 2018 Nov 17 [Epub ahead of print]
28. Nerad E, Lambregts DM, Kersten EL, et al. MRI for local staging of colon cancer: can MRI become the optimal staging modality for patients with colon cancer? *Dis Colon Rectum* 2017; 60:385–392
29. Matsuda I, Akahane M, Sato J, et al. Precision of the measurement of CT numbers: comparison of dual-energy CT spectral imaging with fast kVp switching and conventional CT with phantoms. *Jpn J Radiol* 2012; 30:34–39
30. Wang L, Liu B, Wu XW, et al. Correlation between CT attenuation value and iodine concentration in vitro: discrepancy between gemstone spectral imaging on single-source dual-energy CT and traditional polychromatic X-ray imaging. *J Med Imaging Radiat Oncol* 2012; 56:379–383
31. Miles KA. Tumour angiogenesis and its relation to contrast enhancement on computed tomography: a review. *Eur J Radiol* 1999; 30:198–205
32. Zenk J, Bozzato A, Steinhart H, Greess H, Iro H. Metastatic and inflammatory cervical lymph nodes as analyzed by contrast-enhanced color-coded Doppler ultrasonography: quantitative dynamic perfusion patterns and histopathologic correlation. *Ann Otol Rhinol Laryngol* 2005; 114:43–47
33. Naresh KN, Nerurkar AY, Borges AM. Angiogenesis is redundant for tumour growth in lymph node metastases. *Histopathology* 2001; 38:466–470
34. Mogoantă SS, Calotă F, Vasile I, et al. Histological and immunohistochemical study on sentinel lymph node in colorectal cancer: values and limitations. *Rom J Morphol Embryol* 2016; 57:65–74
35. Al-Najami I, Beets-Tan RG, Madsen G, Baatrup G. Dual-Energy CT of rectal cancer specimens: a CT-based method for mesorectal lymph node characterization. *Dis Colon Rectum* 2016; 59:640–647
36. Cui Z, Gao Y, Wang W, Zhu Z, Zhang Y, Ma Z. Evaluation of neck lymph node metastasis on contrast-enhanced ultrasound: an animal study. *Clin Exp Otorhinolaryngol* 2017; 10:109–114
37. Papadakis AE, Damilakis J. Fast kVp-switching dual energy contrast-enhanced thorax and cardiac CT: a phantom study on the accuracy of iodine concentration and effective atomic number measurement. *Med Phys* 2017; 44:4724–4735

FOR YOUR INFORMATION

A data supplement for this article can be viewed in the online version of the article at: www.ajronline.org.